Variational calculation for the direct-gap exciton in the Ge quantum well systems

Yu-Hsuan Kuo* and Yin-Shun Li
The Graduate Institute of Electronics Engineering, National Taiwan University, Taipei 10617, Taiwan
and Department of Electrical Engineering, National Taiwan University, Taipei 10617, Taiwan
(Received 25 March 2009; revised manuscript received 19 May 2009; published 25 June 2009)

The variational method based on the two-dimensional (2D), three-dimensional (3D), and anisotropic 3D exciton models is used to investigate the ground-level direct-gap electron-heavy-hole exciton behaviors in the Ge quantum well systems, including an infinite Ge well case and a Ge/SiGe finite well case. The exciton radius, binding energy, and oscillator strength are calculated for various well thicknesses and bias voltages. The three exciton models are compared indicating that the dimensionality in the exciton model is nearly 2D for the thin finite well and 3D with anisotropic exciton radiuses for the infinite well and thick finite well. The exciton radius minimum and oscillator strength maximum occur at 1.6 nm well for the finite well case, thus proving that this Ge/SiGe quantum well system possesses strong quantum confinement, even with a thin-well thickness. Also, the effect of the conduction-band nonparabolicity effect on the exciton behavior is discussed. The variational calculation agrees well with the experimental results and other theoretical calculations in the 10 nm finite well case.

DOI: 10.1103/PhysRevB.79.245328 PACS number(s): 78.67.De, 71.35.Cc, 73.21.Fg, 78.20.Bh

I. INTRODUCTION

The photonic devices based on optical absorption are useful for optical modulation and photodetection, which can enable information technologies such as optical communication, optical interconnects, and optoelectronic integrated circuits.[1,2] The electroabsorption effect, especially the quantum-confined Stark effect (QCSE),[3,4] is the strongest optical modulation mechanism, as compared to other methods such as electro-optic or thermo-optic effects, available in the silicon-compatible material system. The strong QCSE electroabsorption effect had been demonstrated in the Ge/SiGe quantum well structures on silicon substrates.[5–8] The direct band-edge excitonic absorption is utilized to achieve the electric-field-dependent changes in absorption-edge wavelength and coefficient, leading to the modulation of the optical absorption and light intensity passing through the quantum well region.[9] Optical modulators with a sub-1 V low-operation voltage swing had been realized.[10] Waveguide photodetectors based on the Ge/SiGe quantum well structure had also achieved the GHz-regime operation.[11] A wider quantum well design and high-temperature operation can shift the absorption edge to the long wavelength region and leverage the benefits of commercial *C*-band (~1530–1565 nm) operation.[6] The theoretical calculation based on the tunneling resonance method was applied to calculate the direct-gap transition energy showing good agreement with experimental results.[5,6,8] The $k.p$ method[7,12] and tight-binding method[13,14] had also been used to calculate the transition energy and optical strength in the Ge/SiGe quantum well system giving good explanations to the photocurrent, transmission, and photoluminescence spectra.[5–7,13,14] Besides, the variational method—a widely used method in the evaluation of the exciton effect and its influence in the QCSE for the III-V and II-VI systems—had been used with a one-variational-parameter exciton model to calculate the exciton radius, binding energy, and optical oscillator strength for the Ge/SiGe quantum well system recently.[6,15]

In this paper, we present a detailed investigation on the variational calculation of the direct-band-edge ground-level electron-heavy-hole (e1-hh1) exciton effect in the Ge quantum well systems, including an infinite Ge quantum well and a finite Ge/SiGe quantum well structure. The two-dimensional (2D) exciton, three-dimensional (3D) exciton, and anisotropic 3D exciton models are used to evaluate the exciton effect. The exciton radius, transition energy, binding energy, and optical oscillator strength are calculated for the quantum wells of different thicknesses under various bias voltages (instead of "electric fields" in most cases of the literature). In the infinite well case, the 2D and 3D exciton models show similar results but their discrepancy becomes significant for wider well. In the finite well case, the calculation based on the anisotropic 3D exciton model indicates that the exciton dimensionality is close to 2D for a thin well and becomes larger (anisotropic 3D) for a wide well, but it would not be exactly 3D because of the anisotropic hole effective masses. The strongest exciton effect occurs for the finite Ge/SiGe quantum well at 1.6 nm well thickness, thus proving the strong quantum confinement in this system. The nonparabolicity of the conduction band and its effect on the electron effective mass are also considered in the calculation of the finite well case, and its comparison with the parabolic conduction-band (a constant electron effective mass) case is made for the 10 nm well. Also, the calculation in the oscillator strength gives good agreement with experimental data and other theoretical results in the 10 nm finite well case.

II. EXCITON AND VARIATIONAL MODELING METHOD

The optical absorption in the semiconductor materials can be largely enhanced by the excitonic effect. However, the bulk excitonic effect only exists at low temperature in a high-purity material without strong electric field; otherwise, excitons can easily smear out due to the field ionization of exciton or the weakened Coulomb interaction by the screening

effect. However, the excitonic effect is more pronounced and sustainable in a quantum well system, thus becoming especially critical to the optical absorption and the QCSE. Even though the formation of excitons has negligible influence in the transition energy, it can change the absorption strength through the strong excitonic coupling. The quantum structure can confine carriers in a tight space and increase their interaction probability, thus expediting the optical transition process and enhancing the absorption strength. The confinement is mainly caused by the barrier in the vertical (well growth) direction and by the excitonic effect in the horizontal plane. An electric field across the quantum well can induce the redistribution of carriers in the well and reduce the direct-gap transition energy, thus shifting the absorption spectrum including the redshift of absorption edge and the reduction in absorption strength. The reduced band-edge absorption combined with the redshifted edge can still transform into an increment of absorption coefficient for the wavelength region where the energy is initially lower than the band-gap transition energy, and this longer wavelength region is the typical operation wavelength for optical modulation. Obviously, it is critical to optimize the electroabsorption effect by minimizing the reduction in optical strength while keeping a large shift under an electric field. As compared to the bulk exciton case, the quantum well can increase the field tolerance in the direction of well growth by around 1 order higher, thus increasing the band-edge absorption shift before the excitonic absorption disappears. Hence the study of bias voltage/field here is focused on the applied direction along the well growth direction (i.e., the cross-well voltage).

Two Ge quantum well structures, including an ideal infinite Ge quantum well structure and a single finite Ge/SiGe quantum well, are investigated here. Both Si and Ge are indirect-gap semiconductor materials. The dominating direct-gap transition (Γ_{8v}-Γ_{7c}) energy is 0.8 eV in Ge,[16] and the relevant Γ-point band-gap energy is 4.0 eV in Si.[17] Due to the high band-gap difference, it is feasible to realize strong quantum confinement even with small compositional difference between the well and the barrier in the Si-Ge material system. The $Ge/Si_{0.15}Ge_{0.85}$ structure is chosen here because it is the typical design for various experimental and theoretical investigations in the literature including the original QCSE report.[5] For the finite well case, the valence-band offset is calculated based on the theoretical study in the literature [Eq. (41) of Ref. 18]. The conduction-band offset is the direct-gap energy difference (linearly interpolated between Si and Ge) minus the valence-band offset.

The quantum well structures in both cases are assumed to be grown on the (001)-oriented, Ge-lattice-matched substrates (buffers), thus the Ge well region is unstrained. This can be realized by using either the layer transfer technique or SiGeSn virtual substrates.[19,20] The latter approach can even produce a tensile strain for the Ge well.[20] When a SiGe buffer is used, the compressive strain in the Ge well can increase the Ge direct-gap energy and deteriorates the direct-gap-to-indirect-gap absorption ratio and QCSE performance.[15] This undesired compressive strain can be minimized to nearly zero by reducing the Si content in the buffer layer if the strain-balanced design is not strictly imposed. This is especially practical since only several pairs of quantum wells are required in the waveguide-type modulators that typically have a long optical path. Besides, the SiGe composition in the substrate/buffer material can affect the band-gap energy dramatically, however, it only changes the barrier height slightly and has negligible effect in the quantum well energy and exciton peak shift [Fig. 7(c) of Ref. 6]. Hence the strain effect can be added into the transition energy without changing other results in this study provided that its magnitude is moderate (e.g., the Si content in the buffer/substrate is less than 15%).

The Hamiltonian for a system consisting of an electron and a hole in a quantum well structure is expressed as[4,21,22]

$$H = H_e + H_h + H_{e\text{-}h},$$

$$H_e = \frac{p_{z_e}^2}{2m_e} + V_e(z_e),$$

$$H_h = \frac{p_{z_h}^2}{2m_{h\perp}} + V_h(z_h),$$

$$H_{e\text{-}h} = \frac{p_{\parallel}^2}{2\mu} - \frac{e^2}{4\pi\varepsilon\sqrt{r^2 + (z_e - z_h)^2}}, \tag{1}$$

where z_e and m_e (z_h and $m_{h\perp}$) are the position and effective mass of electron (hole) along the vertical growth axis (z axis), respectively, r and μ are the relative distance and reduced mass of the electron and hole in the horizontal x-y plane, V_e (V_h) is the potential (including the barrier height and electric-field effect) for the electron (hole), and p is the momentum operator (note that $p_{\parallel}$ includes the radial and angular components in the cylindrical coordinate). The first two terms, H_e and H_h, give the independent Hamiltonians for the electron and hole, respectively, which are actually adequate enough to predict the quantum well energy, transition energy, and wave functions along the growth direction. However, the last Hamiltonian, $H_{e\text{-}h}$, gives the exciton binding effect caused by the Coulomb interaction and relative motion, which can change the probability density of exciton as a function of relative distance, especially in the horizontal plane, and is critical to the enhancement of the optical absorption.

For the conduction band, the electron effective masses at the relevant Γ points are $0.156m_o$ and $0.041m_o$ for Si and Ge, respectively.[23] For the finite well case, the nonparabolicity effect in the conduction band is also considered, which can modify the electron effective mass into

$$m_e'(E_K) = m_e\left(1 + \frac{E_K}{E_{\mathrm{NP}}}\right), \tag{2}$$

where E_K is the energy of the electron above $V_e(z_e)$, and E_{NP} is a material-dependent fitting parameter of nonparabolicity.[8,24] The implementation of nonparabolicity effect in the tunneling resonance simulation can be found in Refs. 8 and 24, and the value of E_{NP} is adopted to be 0.8 eV here. Also, the electron effective mass is assumed to be isotropic here and has the same mass enhancement in the vertical and horizontal directions. The effect of nonparabolicity,

the anisotropy of electron mass, and the comparison between the parabolicity and nonparabolicity assumptions will be discussed in the end of the next section. For the valence band, the quantum well structure breaks the heavy-hole or light-hole degeneracy. The heavy-hole band becomes the topmost valence band and dominates the band-edge optical absorption, thus the investigation is focused on the heavy hole. The heavy-hole effective masses are $0.49m_o$ and $0.28m_o$ for bulk Si and Ge, respectively.[25] However, the quantum well also breaks the centrosymmetry of valence-band structure to the Γ point, thus the hole effective mass becomes anisotropic. The heavy-hole effective masses are calculated based on the Luttinger parameters, giving $0.291m_o$ and $0.21m_o$ ($0.216m_o$ and $0.057m_o$) for $m_{hh\perp}$ (and $m_{hh\parallel}$) of Si and Ge, respectively.[6] The effective masses of SiGe are linearly interpolated between those of Si and Ge. The dielectric constant, $\varepsilon/\varepsilon_o$, is 16 for the Ge well (and also the SiGe barrier) where ε_o is the permittivity in vacuum, so the electric fields in the well and the barrier are the same under a bias voltage for the simplicity of calculation in the finite well case.

The uncoupled wave functions, $\psi_e(z_e)$ and $\psi_h(z_h)$, of ground-level electrons and heavy holes are evaluated separately based on their respective Hamiltonians, H_e and H_h. The wave functions in the finite well case are evaluated numerically with the tunneling resonance method using 10 nm barriers and 0.05 nm segment. The wave functions in the infinite well of thickness L are solved analytically[4,26] by defining a new variable

$$Z = -\left(\frac{2m}{(e\hbar F)^2}\right)^{1/3}(E + qFz) \tag{3}$$

and using the Airy functions A_i and B_i for wave equation

$$\psi(z) = aA_i(Z) + bB_i(Z), \tag{4}$$

where q is the carrier charge, F is the bias field, and m is the carrier effective mass. The ratio of coefficients a/b and the ground-level energy E can be found by solving

$$\psi\left(z = \frac{+L}{2}\right) = \psi\left(z = \frac{-L}{2}\right) = 0. \tag{5}$$

The variational method is used here to evaluate the excitonic coupling between the electron and hole. A Bohr-atom-like $1s$ model is widely used to form the complete coupled wave function in various forms,[3,4,21,22,26–32] and the following trial equation is used here to minimize the total system energy based on the complete Hamiltonian H (Refs. 22, 26, and 29–32):

$$\Psi(z_e, z_h, r) = \psi_e(z_e)\psi_h(z_h)\exp[-\sqrt{\alpha^2 r^2 + \beta^2(z_e - z_h)^2}]$$
$$= \psi_e(z_e)\psi_h(z_h)\exp\left[-\frac{\sqrt{r^2 + \eta(z_e - z_h)^2}}{\lambda}\right], \tag{6}$$

where (α, β) and (λ, η) are two equivalent sets of variational parameters, λ is $1/\alpha$, and η is $(\beta/\alpha)^2$. The optimized values of $1/\alpha$ and $1/\beta$ represent the exciton radiuses in the horizontal plane and vertical direction,[22,26] while those of λ and η are the exciton radius and dimensionality,[30–32] respectively. It should be also noted that the dimensionality originally defined in Ref. 29 has a power of 2, which gives a more meaningful horizontal/vertical exciton radius ratio (β/α). Here the second form of the complete trial wave function based on the variational parameters, λ and η, is used for the calculation. For the traditional 2D and 3D models, the exciton in the vertical z direction is either neglected ($\beta = \eta = 0$) or assumed to have the same radius as the horizontal size ($\alpha = \beta = 1/\lambda$, $\eta = 1$). For the anisotropic 3D exciton model, the value of η can be different from zero or unity, so the exciton radius becomes anisotropic with different sizes in the z direction and x-y plane. All three models are being used here to investigate the excitonic effects.

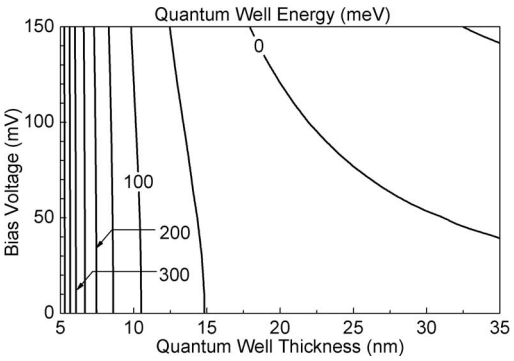

FIG. 1. Contour plot of the ground-level quantum well energy (the combined energy of independent direct-gap electron and hole) versus the well thickness and bias voltage in the infinite Ge quantum well.

Besides the $1s$ exciton state, other discrete and continuous states also exist for the ground-level electron and heavy hole (analogous to the infinite states in the Bohr model) and it is difficult to resolve the absorption peaks between them due to their small energy difference (in the magnitude of meV) at room temperature. However, the main excitonic peak of $1s$ located at the absorption edge is still easy to observe in a quantum well structure, which dominates the practical efficiency of excitonic absorption devices. The excitonic absorption enhancement can be evaluated through the optical oscillator strength, which is proportional to the square of normalized overlap integral of electron and hole states:

$$I \propto \frac{\langle\psi_e|\psi_h\rangle^2}{\langle\Psi|\Psi\rangle}, \tag{7}$$

thus the strong coupling of the electron-hole wave function through the well confinement and excitonic attraction can increase the absorption significantly.

III. RESULTS

A. Infinite Ge quantum well structure

The wave functions of ground-level electron and heavy hole are first calculated without considering the exciton effect and the combined quantum well energy is shown in Fig. 1. The quantum well energy in an ideal infinite quantum well can also be calculated using the second-order perturbation method leading to a fourth-power dependence in the well thickness and a quadratic dependence in the field, or both

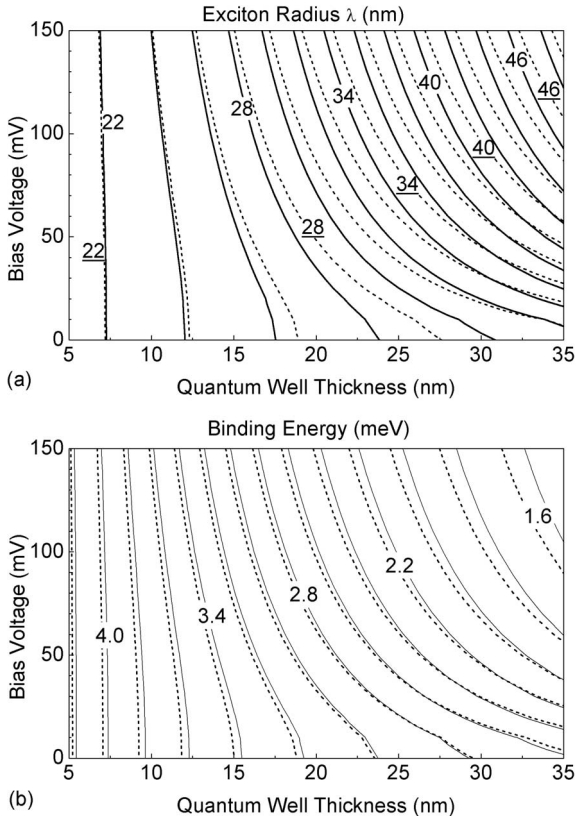

FIG. 2. Contour plots of (a) exciton radius and (b) binding energy for varying well thickness and bias voltage in the infinite Ge quantum well using the 2D (solid line) and 3D models (dashed line). The discrepancy is less than 10% in the radius and less than 0.1 meV in the binding energy.

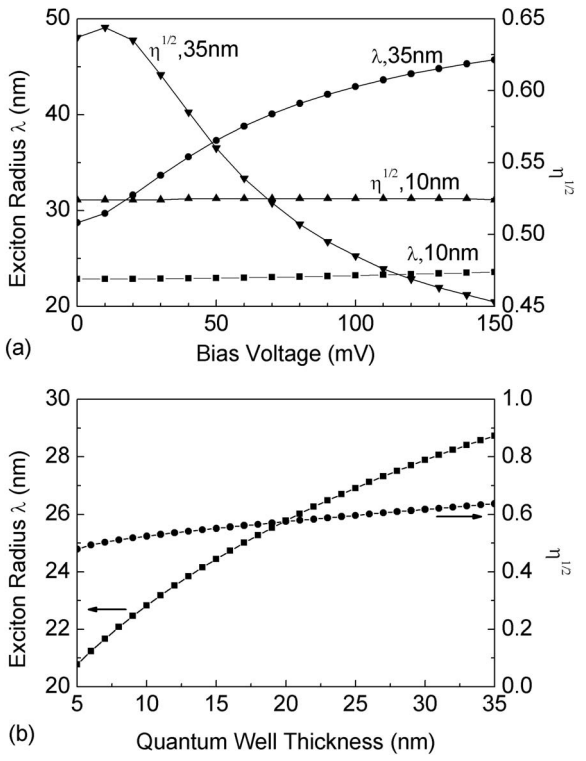

FIG. 3. The exciton radius (λ) and dimensionality (in the form of $\eta^{1/2}$) as functions of (a) bias voltage (for the 10 and 35 nm wells) and (b) well thickness (under zero-bias voltage) in the infinite Ge quantum well.

quadratic dependences in the well thickness and bias voltage, which agrees with the trend here. It should be noted that the comparison is based on the "cross-well voltage" here instead of the "electric field," even though the latter one is commonly used in the literature. In this case, the voltage concept gives relatively similar energy shift for different quantum well thickness (though the quadratic voltage dependence still moves a thicker well more than a thinner well under the same voltage). This also gives fair comparison to evaluate the performance for modulator applications, which prefers a larger redshift in wavelength (caused by quantum well energy reduction) and a higher exciton absorption strength.

Next, we consider the exciton binding using the one-variational-parameter exciton models. Figures 2(a) and 2(b) show the contour plots of exciton radius as well as the binding energy, respectively, in an infinite Ge quantum well based on the 2D and 3D models as a function of well thickness and cross-well bias voltage. The exciton radius increases with higher voltage and thicker well in both models, owing to the weaker binding in a wide well and the field ionization of exciton. The 2D exciton radius is slightly larger than the 3D one and the discrepancy increases with thicker well but is still less than 10%. In the 2D exciton case, the bias voltage/field along the growth direction has no direct effect in the variational parameter λ, which only determines the electron-hole distance in the horizontal plane, but the voltage can still affect λ indirectly through the voltage-dependent z-directional wave function distribution. In the 3D case, the variational parameter can affect the spacing along growth direction and change the potential, thus the discrepancy between the 2D and 3D models becomes larger. The total transition energy of ground-level direct-gap absorption is the combination of direct-gap energy and the quantum well energy (in Fig. 1) minus the exciton binding energy. The binding energy, ranging from ~1.4 to ~4.2 meV, reduces with increasing exciton radius. The energy for the 2D model is slightly higher than that of the 3D model except for the thicker wells (> ~27 nm) with low bias voltage; however, the difference between these two limiting cases is less than 0.1 meV.

The anisotropic 3D exciton model with two variational parameters can further minimize the total system energy (i.e., maximize the binding energy). The binding energy increases and then decreases with the dimensionality, thus the optimal dimensionality occurs at neither 0 (2D) nor 1 (3D) but has an intermediate value. The energy difference caused by varying dimensionality is typically less than 0.1 meV in this system. Figure 3(a) shows the exciton radius and dimensionality (in the form of $\eta^{1/2}$) under various bias voltages for the 10 and 35 nm infinite wells. For the thin well, the dimensionality and radius have negligible changes with bias voltage. For the thick well, the dimensionality decreases and the radius increases with higher bias voltage leading to a larger exciton size in both horizontal and vertical directions. Comparing Figs. 2(a) and 3(a), the exciton radius in the anisotropic 3D

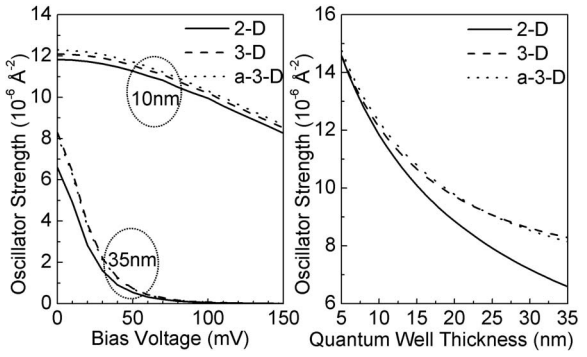

FIG. 4. The voltage dependence (for the 10 and 35 nm wells) and well-thickness dependence (under zero-bias voltage) of oscillator strength in the infinite Ge quantum well using the 2D (solid line), 3D (dashed line), and anisotropic 3D models (dotted line). The curves of the 3D and anisotropic 3D models are nearly identical.

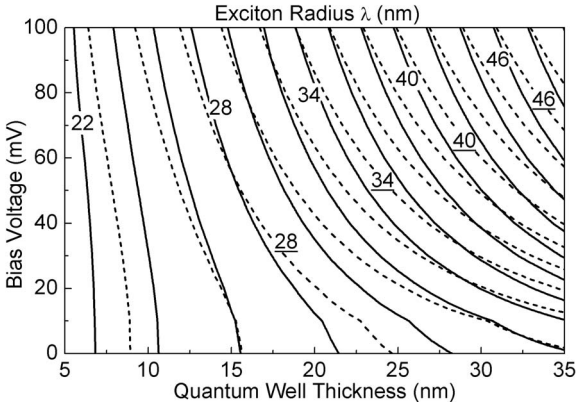

FIG. 5. Contour plots of the exciton radius for varying well thickness and bias voltage in the finite $Ge/Si_{0.15}Ge_{0.85}$ quantum well using the 2D (solid line, number without underline) and 3D (dashed line, number with underline) models.

model is close to those in the 2D and 3D models. Figure 3(b) shows that both the exciton radius and dimensionality under zero-bias voltage/field increase with the well thickness in our chosen range, and it is expected that these parameters will finally approach the bulk exciton values. For a thin well, the electron-hole separation in the z direction is much smaller than the vertical exciton size, thus the inclusion or exclusion of the vertical exciton radius (or dimensionality) in the calculation would yield similar results. However, for a thicker well, the 3D or anisotropic 3D models can give stronger binding in the z direction and better approximation to the real exciton. The results here agree well with the investigation of the infinite quantum well system under zero bias in the literature[22] and we expect that the dimensionality in Fig. 3(b) would increase if we extend the well thickness. But it should be noted that the hole effective mass here is anisotropic ($m_{hh\perp}$ is heavier than $m_{hh\parallel}$), thus the value of η would not exactly be 1.

Figure 4 shows the voltage dependence (for two specific 10 and 35 nm wells) as well as the well-thickness dependence (under zero-bias voltage) of the oscillator strength based on the 2D, 3D, and anisotropic 3D models. When the infinite quantum well is unbiased, the square quantum well gives an identical cosine-distributed wave function to the ground-level carriers leading to a perfect z-directional overlap. Thus the oscillator strength is determined solely by the choice of exciton model as well as the optimal exciton radius: the strength is inversely proportional to the square of exciton radius in the 2D model and a similar trend can be found in the 3D and anisotropic 3D models. When the well is electrically biased, the oscillator strength reduces, partially contributed by the reducing original z-directional overlap and partially caused by a wider exciton. The results shown in Fig. 4 are similar to all three models, especially for the thin well (where the inclusion of z-directional coupling by the exciton is not critical) as well as thick well under high bias (where the decoupling of electron and hole gives a low strength). The 3D and anisotropic 3D models show nearly identical curves. The main discrepancy occurs for the thick wells where the 2D model underestimates the exciton coupling in the z direction than other two models. The oscillator strengths of the 20 and 35 nm wells in the 3D models are 10% (15%) and 26% (29%) higher than those in the 2D model under zero- (150 mV) bias voltage, respectively.

B. Finite Ge/SiGe quantum well system

The modeling conditions for the finite well case here are similar to those of the infinite well case, except that the nonparabolicity effect on the electron effective mass is considered and the bias voltage across the "well" is limited to 100 mV (close to the barrier height of the valence band) instead of 150 mV. This 100 mV bias voltage variation can produce a QCSE shift of 17, 19, 31, and 44 meV for 5, 10, 20, and 35 nm finite wells, respectively. This shift is stronger than the infinite well and adequate for the QCSE modulator applications (the wavelength shift expressed in nm is nearly double of the energy shift expressed in meV for this wavelength region).

Figure 5 show the exciton radius for the two limiting cases, the 2D and 3D models. The exciton radius ranges from 20.78 (22.09 nm) to 50.07 nm (49.95 nm) for the 2D (3D) case. The radius difference between the two models is less than 1 nm for the well of thickness ranging from around 8 to 22 nm, but the discrepancy is relatively larger than the infinite case. Comparing the results between the finite well (Fig. 5) and the infinite well [Fig. 2(a)], the trend and magnitude are similar. But the exciton radius is larger for the finite well case (except for the ultrathin-well region where the nonparabolicity effect is strong) leading to a weaker exciton binding. This mainly comes from the weaker confinement of the finite barriers, thus causing the "leak" of carriers into the barriers, especially under high bias voltage. And hence a thinner finite well has a similar result as a thick infinite well (a larger effective thickness).

Figure 6(a) shows the exciton parameters (λ, $\eta^{1/2}$) under various bias voltages for the 10 and 35 nm finite wells. Under a higher bias voltage, the exciton radius increases while the dimensionality decreases slightly, but the change for the 10 nm well is not significant. Figure 6(b) shows that the exciton radius and dimensionality ($\eta^{1/2}$) increase with well

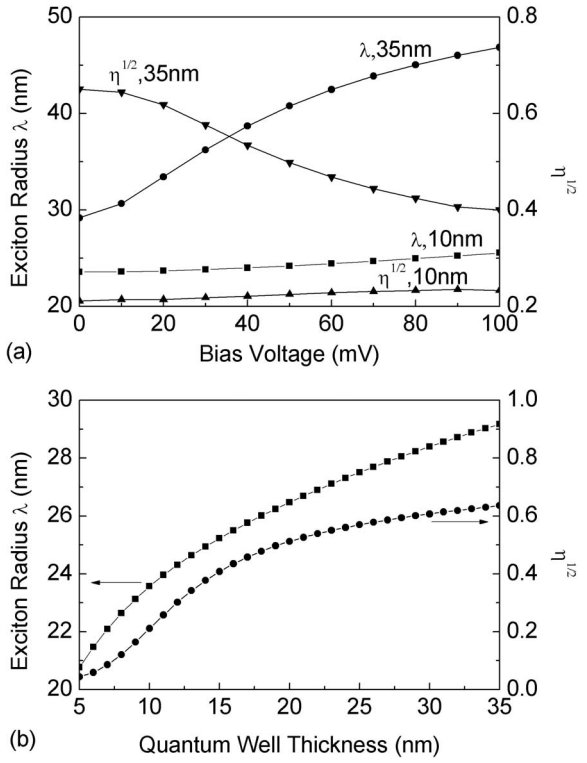

FIG. 6. The exciton radius (λ) and dimensionality (in the form of $\eta^{1/2}$) as functions of (a) bias voltage (for the 10 and 35 nm wells) and (b) well thickness (under zero-bias voltage) in the finite $Ge/Si_{0.15}Ge_{0.85}$ quantum well.

thicknesses under zero-bias voltage. The value of $\eta^{1/2}$ is nearly zero (0.044) for the 5 nm well (2D exciton) and finally approaches 0.63 for the 35 nm well. Comparing Figs. 3(b) and 6(b), the variation in dimensionality here is much dramatic than that of the infinite case while the difference of exciton radius between two cases is not significant (less than 1 nm). The low dimensionality in the thin-well region is different from the results calculated in some finite well cases based on III-V (InGaAs/GaAs)[31] or II-VI (CdTe)[30] compounds where the dimensionality takes an intermediate value, but the trends of thickness and field dependences are similar. Besides, the dimensionality in Ref. 29 is also close to zero for the $GaAs/Al_{0.4}Ga_{0.6}As$ and $InP/In_{0.53}Ga_{0.47}As$ finite wells of thickness ranging from ~1 to 20 nm.

Figures 7 and 8 show the exciton binding energy and optical oscillator strength, respectively, for the finite wells based on the 2D, 3D, and anisotropic 3D models. Both values are important indicators of exciton strength and reduce with higher bias voltage and thicker well. The discrepancy in the binding energy between the 3D model and the 2D (or anisotropic 3D) model is obvious for the thin-well region, and this difference has no significant change for various bias voltages (the curves of 10 nm well under various bias). The maximum difference of 0.3 meV occurs for the 5 nm well. For the oscillator strength, the 3D model is close to the anisotropic 3D model for the thin-well (under high bias voltage) and thick-well regions. Also, the difference between three models decreases with higher bias voltage. Under zero-bias voltage, the oscillator strength of the anisotropic 3D

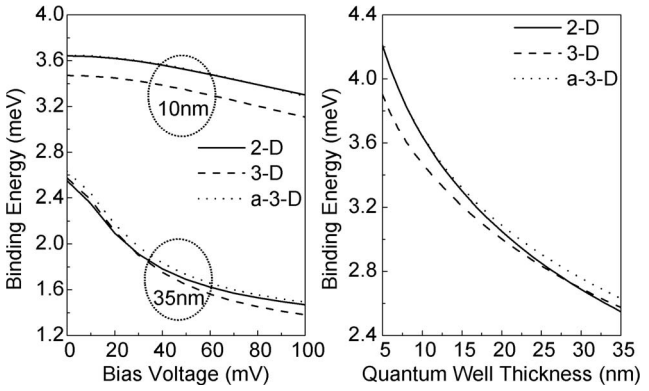

FIG. 7. The voltage dependence (for the 10 and 35 nm wells) and well thickness dependence (under zero-bias voltage) of binding energy in the finite $Ge/Si_{0.15}Ge_{0.85}$ quantum well using the 2D (solid line), 3D (dashed line), and anisotropic 3D models (dotted line).

case can be fitted by the 2D and 3D curves when choosing the one with higher value for each thickness. Apparently, the discrepancy between the 2D, 3D, and anisotropic 3D models here becomes more significant than that of the infinite well, but the difference is still less than ~15% in the oscillator strength. It is common to use a one-variational-parameter model to evaluate the exciton effect in order to reduce the calculation load. Since the 3D model is close to the anisotropic model for the thick-well region where the z-directional exciton coupling should be considered, it is a suitable choice for the investigation of wide thickness range. If the thickness range is below ~10 nm, then the 2D model gives better approximation.

One key difference between the finite well and infinite well is the trend of exciton radius versus quantum well thickness. For the infinite well, the exciton radius reduces monotonically with thinner well. For the finite well, a minimum of exciton radius should be observed. Thus the well thickness range is extended to nearly zero in Fig. 9 to investigate this effect under zero-bias voltage, using the 2D model and analytical wave function solutions. The radius minimum (and

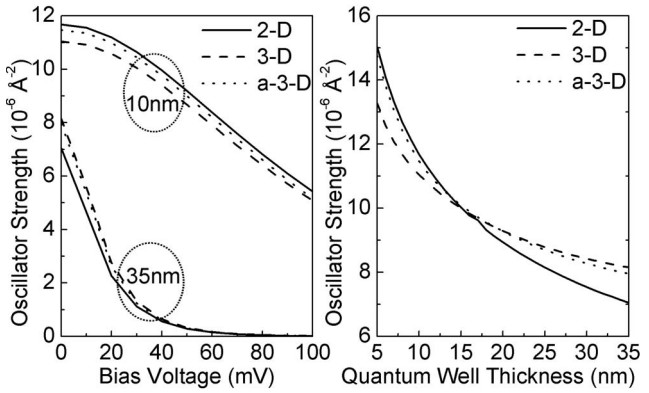

FIG. 8. The voltage dependence (for the 10 and 35 nm wells) and well thickness dependence (under zero-bias voltage) of oscillator strength in the finite $Ge/Si_{0.15}Ge_{0.85}$ quantum well using the 2D (solid line), 3D (dashed line), and anisotropic 3D models (dotted line).

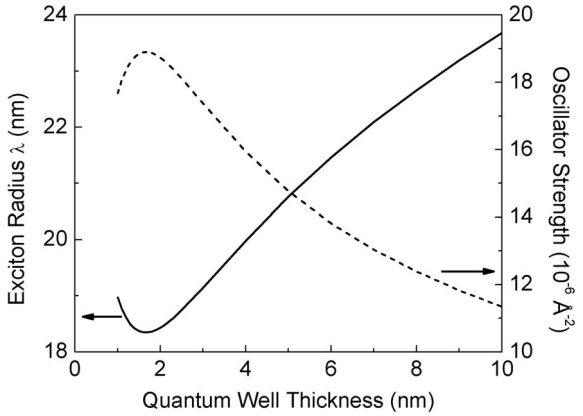

FIG. 9. The exciton radius and oscillator strength as functions of well thickness in the $Ge/Si_{0.15}Ge_{0.85}$ quantum well using the 2D model. The radius minimum (and the oscillator strength maximum) occurs at the 1.6 nm well.

the oscillator strength maximum) occurs at the 1.6 nm well, whose oscillator strength (and exciton radius) is 1.67 (0.77) times that of the 10 nm well (noted that 1.67 is close to $1/0.77^2$). The thickness of well with the strongest exciton effect is a relatively small value as compared to the GaAs/AlGaAs or InGaAs systems[27,29] proving the strong quantum confinement in this $Ge/Si_{0.15}Ge_{0.85}$ quantum well system.

The effective masses can affect the wave function distribution, quantum well energy, exciton energy, and oscillator strength, thus the use of different mass parameters might change the modeling significantly. Figure 10 shows the comparison between the use of the parabolicity and nonparabolicity effects in the conduction band for 10 nm well versus bias voltage using the 3D model. With the nonparabolicity effect, the electron effective mass becomes ~5% heavier and also causes a heavier horizontal reduced mass (μ). This results in a reduction (~3%) in the quantum well energy and Stark shift, a smaller exciton radius (~5%), and higher oscillator strength (~10%, nearly inverse proportional to the

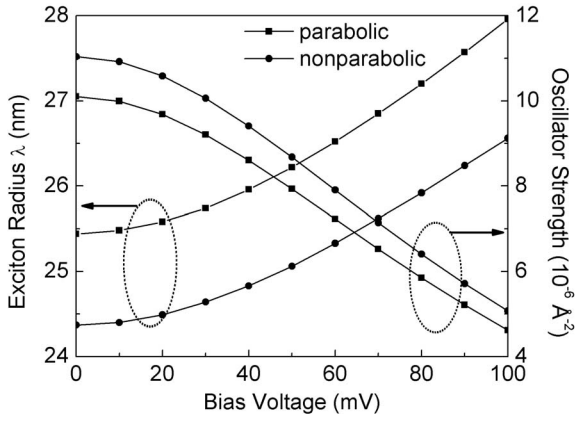

FIG. 10. Comparison between different electron effective masses (the parabolicity versus nonparabolicity assumptions for the conduction band) based on a 10 nm finite well. The exciton radius and oscillator strength are calculated as functions of bias voltage using the 3D model. The enhancement of electron effective mass is assumed to be isotropic here.

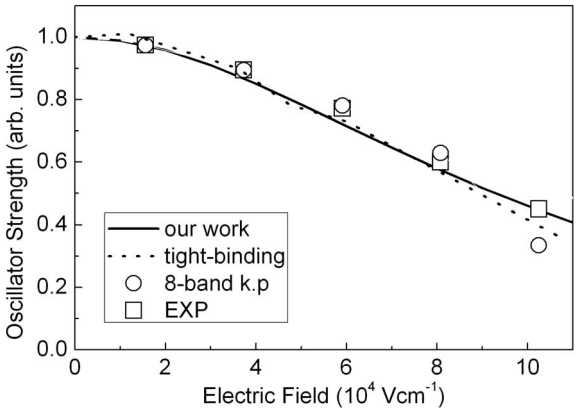

FIG. 11. The oscillator strength from our work (anisotropic 3D model), experimental data (Ref. 5), and other theoretical results [the eight-band $k.p$ method (Ref. 12) and the tight-binding method (Ref. 14)] for the 10 nm finite well case. The oscillator strength is normalized to the zero-field value. The oscillator strength and the squared matrix element are nearly proportional to the peak absorption coefficient. Our calculation agrees well with the experimental measurement and other theoretical results.

square of exciton radius), and the trend has no significant change for various bias voltages. The difference caused by the nonparabolicity effect in the 10 nm well is observable but not significant; if the quantum well becomes thinner (thicker), the electron effective mass will increase (decrease) causing more (less) difference. Obviously, the inclusion of the nonparabolicity effect can enhance the exciton strength in an ultrathin well based on a low-gap material such as Ge, which is actually contributed by the mass enhancement in the horizontal plane. The theoretical calculation and cyclotron mass measurement (in the GaAs/AlGaAs well) indicate that the existence of anisotropy in the nonparabolic conduction band gives a stronger enhancement (~2–3×) for the horizontal mass (relative to its bulk value) than the vertical mass.[33] Even though there are uncertainties in the fitting parameter E_{NP} and the ratio of the anisotropic horizontal/vertical mass enhancement for Ge, our conservative assumption of an isotropic enhancement in the electron effective mass would not overestimate for the strong exciton effect and quantum confinement (i.e., the small radius minimum in Fig. 9) in this quantum well system.

Our theoretical calculation is compared with the experimental data from the original, widely studied 10 nm finite well case[5] and other theoretical calculations[12,14] as well. Since the Stark shift of the exciton peak dominated by the change in quantum well energy had been well explained by the tunneling resonance method,[5,6,8] here we focus the comparison on the band-edge absorption coefficient, which is proportional to the optical oscillator strength (or the squared dipole matrix element). Figure 11 shows the relative optical oscillator strength, normalized to the zero-field value, from the experimental measurement and theoretical calculations, which indicates good agreement between our work and previous results. It should be noted that the experimental absorption coefficient also includes the indirect-gap absorption, which is not considered in our direct-gap exciton calculation, thus the experimental result is slightly higher than our work.

IV. CONCLUSIONS

The variational method is used to investigate the exciton effect in the infinite Ge quantum well and the finite $Ge/Si_{0.15}Ge_{0.85}$ quantum well cases. The calculation based on the one-variational-parameter 2D and 3D models as well as the two-variational-parameter anisotropic 3D model show similar trends and results in the exciton radius, binding energy, and oscillator strength. For the ideal infinite well case, the 3D model is close to the most accurate anisotropic 3D model, and their discrepancy with the 2D model becomes more significant for the thick wells owing to the inclusion/exclusion of z-directional exciton binding. Also, the dimensionality ($\eta^{1/2}$) has an intermediate value. For the finite $Ge/Si_{0.15}Ge_{0.85}$ well case, the 3D model is close to the anisotropic 3D model for the thick-well or high-voltage conditions. The exciton dimensionality has a relatively significant change from 2D to anisotropic 3D as the well thickness increases, but the ultimate value of $\eta^{1/2}$ would not be unity owing to the anisotropic hole effective mass. If only the one-variational-parameter model can be used, the 3D model is suitable for the thick wells or a study covering a wide thickness range and the 2D model is suitable for the thin wells (less than $\sim$10 nm). The exciton radius minimum and oscillator strength maximum occur at 1.6 nm for the Ge/SiGe quantum well indicating the strong quantum confinement for this quantum well system. The comparison of inclusion/exclusion of the nonparabolicity effect is discussed and the difference becomes more significant for the thin-well case. Also, the variational calculation provides good agreement with experimental and other theoretical results for the widely studied 10 nm finite well case.

ACKNOWLEDGMENTS

The authors would like to acknowledge the grant support from National Science Council under Project No. NSC-96-2221-E-002-267-MY3. We are also grateful to Computer and Information Networking Center, National Taiwan University for the support of high-performance computing facilities.

*Corresponding author; yhkuo@cc.ee.ntu.edu.tw

[1] D. A. B. Miller, Proc. IEEE **88**, 728 (2000).
[2] R. A. Soref, Proc. IEEE **81**, 1687 (1993).
[3] D. A. B. Miller, D. S. Chemla, T. C. Damen, A. C. Gossard, W. Wiegmann, T. H. Wood, and C. A. Burrus, Phys. Rev. Lett. **53**, 2173 (1984).
[4] D. A. B. Miller, D. S. Chemla, T. C. Damen, A. C. Gossard, W. Wiegmann, T. H. Wood, and C. A. Burrus, Phys. Rev. B **32**, 1043 (1985).
[5] Y.-H. Kuo, Y. K. Lee, Y. Ge, S. Ren, J. E. Roth, T. I. Kamins, D. A. B. Miller, and J. S. Harris, Nature (London) **437**, 1334 (2005).
[6] Y.-H. Kuo, Y. K. Lee, Y. Ge, S. Ren, J. E. Roth, T. I. Kamins, D. A. B. Miller, and J. S. Harris, IEEE J. Sel. Top. Quantum Electron. **12**, 1503 (2006).
[7] S. Tsujino, H. Sigg, G. Mussler, D. Chrastina, and H. von Känel, Appl. Phys. Lett. **89**, 262119 (2006).
[8] R. K. Schaevitz, J. E. Roth, S. Ren, O. Fidaner, and D. A. B. Miller, IEEE J. Sel. Top. Quantum Electron. **14**, 1082 (2008).
[9] J. E. Roth, O. Fidaner, R. K. Schaevitz, Y.-H. Kuo, T. I. Kamins, J. S. Harris, Jr., and D. A. B. Miller, Opt. Express **15**, 5851 (2007).
[10] J. E. Roth, O. Fidaner, E. H. Edwards, R. K. Schaevitz, Y.-H. Kuo, N. C. Helman, T. I. Kamins, J. S. Harris, and D. A. B. Miller, Electron. Lett. **44**, 49 (2008).
[11] O. Fidaner, A. K. Okyay, J. E. Roth, R. K. Schaevitz, Y.-H. Kuo, K. C. Saraswat, J. S. Harris, and D. A. B. Miller, IEEE Photon. Technol. Lett. **19**, 1631 (2007).
[12] D. J. Paul, Phys. Rev. B **77**, 155323 (2008).
[13] M. Bonfanti, E. Grilli, M. Guzzi, M. Virgilio, G. Grosso, D. Chrastina, G. Isella, H. von Känel, and A. Neels, Phys. Rev. B **78**, 041407(R) (2008).
[14] M. Virgilio and G. Grosso, Phys. Rev. B **77**, 165315 (2008).
[15] Y.-H. Kuo and Y.-S. Li, Appl. Phys. Lett. **94**, 121101 (2009).
[16] W. C. Dash and R. Newman, Phys. Rev. **99**, 1151 (1955).
[17] D. E. Aspnes and A. A. Studna, Solid State Commun. **11**, 1375 (1972).
[18] S. Galdin, P. Dollfus, V. Aubry-Fortuna, P. Hesto, and H. J. Osten, Semicond. Sci. Technol. **15**, 565 (2000).
[19] R. A. Soref and C. H. Perry, J. Appl. Phys. **69**, 539 (1991).
[20] J. Menéndez and J. Kouvetakis, Appl. Phys. Lett. **85**, 1175 (2004).
[21] G. Bastard, E. E. Mendez, L. L. Chang, and L. Esaki, Phys. Rev. B **26**, 1974 (1982).
[22] Y. Shinozuka and M. Matsuura, Phys. Rev. B **28**, 4878 (1983); **29**, 3717 (1984).
[23] M. Cardona and F. H. Pollak, Phys. Rev. **142**, 530 (1966).
[24] P. J. Stevens, M. Whitehead, G. Parry, and K. Woodbridge, IEEE J. Quantum Electron. **24**, 2007 (1988).
[25] S. M. Sze, *Physics of Semiconductor Devices*, 2nd ed. (Wiley, New York, 1981).
[26] M. Matsuura and T. Kamizato, Phys. Rev. B **33**, 8385 (1986).
[27] R. L. Greene, K. K. Bajaj, and D. E. Phelps, Phys. Rev. B **29**, 1807 (1984).
[28] J. A. Brum and G. Bastard, Phys. Rev. B **31**, 3893 (1985).
[29] M. Grundmann and D. Bimberg, Phys. Rev. B **38**, 13486 (1988).
[30] R. Andre, J. Cibert, and L. S. Dang, Phys. Rev. B **52**, 12013 (1995).
[31] P. Ballet, P. Disseix, J. Leymarie, A. Vasson, A.-M. Vasson, and R. Grey, Phys. Rev. B **56**, 15202 (1997).
[32] C. Monier, A. Freundlich, and M. F. Vilela, J. Appl. Phys. **85**, 2713 (1999).
[33] U. Ekenberg, Phys. Rev. B **40**, 7714 (1989).